

DOPING EFFECT OF Sm ON THE ENERGY GAP AND OPTICAL DISPERSION OF a-Se

M. F. KOTKATA*, M.S. AL-KOTB, F. A. ABDEL-WAHAB

Semiconductors Technology Lab., Faculty of Science, Ain Shams University, Cairo -11566, Egypt

The optical transmission $T(\lambda)$ as well as the reflection $R(\lambda)$ spectra has been recorded, in the spectral range of 500-2500 nm, for thermally deposited Sm doped a-Se films. The X-ray diffraction technique was used to critically identify the structural nature of the studied films. The current optical theories and models were applied to analyze the recorded spectra and to calculate various interesting optical parameters. These include: dispersion of the two components of both complex refractive index ($\tilde{n} = n - ik$) and complex dielectric constant (ϵ_1 and ϵ_2), energy gap (E_g), Urbach energy (E_u), single oscillator energy (E_o), lattice oscillating strength (E_l), material dispersion $M(\lambda)$ and the wavelength at zero material dispersion (λ_c). At this point, a similar non-monotonic trend is observed for the compositional dependence of various parameters. This has been ascribed to the disorder and/or structural defects introduced due to the incorporation of Sm, up to 0.008 % Sm, in the a-Se matrix. Besides, a trial has been made thus estimating the inter-band transitions for the Se-Sm samples investigated.

(Received February 12, 2010; accepted February 22, 2010)

Keywords: Non-crystalline semiconductors; chalcogenides; Optical properties; Thin films; Rare-earth-Sm doping a-Se; Sm-Se.

1. Introduction

A wide range of interesting physical properties is expected for the materials' family concerning rare earth chalcogenide semiconductors. In literature, one can find out many reports on the structure and physical properties of single crystals and films for mono-chalcogenides of bivalent rare earth elements (Eu, Yb and Sm). Since the 70th of the last century, pressure-induced semiconductor-metal transitions were observed in samarium (Sm) mono-chalcogenides, (c.f., [1-3] and references cited therein). Such transitions are correlated with the hybridization of the localized 4f-states with the non-localized conduction band states. Detailed studies and knowledge on the energy levels of the 4f-electron excitation spectra have been reported for Sm-monochalcogens, (c.f., [4] and references cited therein).

The most interesting chalcogen is the element selenium. Amorphous Se (a-Se) attracted great attention for more than three decades (see [5-8] and references cited therein). The importance of a-Se originates from its atomic configuration disorder which is accountable for the existence of the localized electronic states within the band gap. The structural disorder made a-Se and its alloys to have a high optical transparency in the visible and infra red (IR) spectral regions. Besides, it has large refractive index and high degree of covalent bonding which results in oscillator strength and radiative transition probabilities greater than in many other materials (c.f., [9]). On the other hand, Sm is characterized by the presence of 4f and 6s states in its atomic configuration ($[Xe] 4f^6 6s^2$). Samarium monoselenide (SmSe) crystallizes in NaCl structure, and at zero pressure the 4f⁶ states of divalent Sm (Sm²⁺) are fully occupied and situated in the energy gap between chalcogen 3p (lone-pair valence band) and Sm 5d states [10]. These 5d states of Sm together with the conduction band of a-Se form the new conduction band of Sm monoselenide. The crystal field of these compounds splits the conduction band into two sub-bands, namely e_g and t_{2g} . The hybridization of

*Corresponding author: mfk.asu@gmail.com

the $4f$ and $6s$ states of Sm locates another sub-band between the two sub-bands t_{2g} and e_g of the conduction band. The external pressure applied to SmSe decreases its lattice constants that is accompanied by an increase in both width of the Sm $4f^6$ - $5d$ bands and the splitting of e_g - t_{2g} bands, [11,12]. At a given pressure, the $4f^6$ states overlaps with the $5d$ bands that lead to first-order valence phase transition [12].

In fact, the doping of a-Se with traces of Sm modifies its structural network and consequently changes its basic physical properties that makes it a promising candidate for optical devices such as highly efficient amplifiers and lasers [13], IR transmitting materials [14] and other various technological applications [15,16]. Viewing the importance of the subject, different techniques were used to prepare Se-Sm, [17-21].

In two previous papers [20,21], the ac and dc electrical conduction mechanism and dielectric relaxation properties of bulk crystalline and amorphous films of $\text{SeSm}_{0.005}$ semiconductor were studied in a wider range of frequency and temperature. The concept of the Meyer-Neldel rule in the expression of the relaxation time was, also, considered for both ac and dc experimental data. The present work aims at discovering the role played by the incorporation of Sm, up to 0.008 %, in the appearance of some interesting optical dispersion properties as well as the energy gap of a-Se.

2. Experimental

Homogeneous massive bulk ingots (3 gms) of pure Se as well as Se doped with Sm (0.005 and 0.008 %) were prepared by the melt-quenching technique. Each quenched ingot was used as a source material to prepare the thin films investigated in this paper. The latter was prepared by the thermal deposition technique at room-temperature ($RT \approx 25^\circ\text{C}$) under a starting pressure of 10^{-6} Torr on quartz substrates using a coater unit of model: Edwards E306A. Details of the bulk and film preparation conditions are given elsewhere [21]. The nature of the structural phase of the as-deposited films were identified using an X-ray diffraction (XRD) computerized system (model: Philips EXPERT-MPDVG PW-3040 diffractometer) with CuK_α radiation of wavelength $\lambda=0.15406$ nm.

Measurements of the transmittance $T(\lambda)$ and the reflectance $R(\lambda)$ were carried out using a computer-aided two-beam spectrophotometer (type: Shimadzu-3101PC UV-VIS-NIR). The function $T=f(\lambda)$ was recorded at normal incidence, and that of $R=f(\lambda)$ was automatically recorded when the incident beam made an angle $5.0 \pm 0.1^\circ$ to the normal of the film surface. A resolution limit of 0.2 nm and a sampling interval of 2 nm are utilized for the different measuring points. Also, the accuracy of measuring $T(\lambda)$ and $R(\lambda)$ is 0.003. The measurements were carried out at RT for the recorded entire spectral range of 500–2500 nm.

3. Results and discussion

3.1. Nature of as-deposited films

The recorded XRD patterns for the studied as-prepared un-doped and the two Sm doped Se films are shown in Fig. 1. In this figure, it is shown that the XRD pattern of the pure Se film (413 nm) is characterized by the absence of any diffraction peaks indicating its complete amorphous nature. The doped Se film with 0.005 at.% Sm (776 nm) reflects an amorphous matrix embedded with some crystalline zones, [21]. Such zones appear through out two characteristic selenium lines lying in the region of the main diffraction hump covering roughly the range of 23-32 in $2\theta^\circ$ angular units. On the contrary, the XRD pattern of the deposited $\text{SeSm}_{0.008}$ film (1140 nm) reflects a crystallized nature composed of mixed phases; these include: elemental Se (111), (100), (101) & (430), elemental Sm (221), (015), (043) & (103), and SeSm with cubic (111) and tetragonal (105) & (103) structures. The former cubic structure of SeSm has been recorded by other authors for Sm monoselenides, [17,22]. Here, one may infer that the main diffraction hump observed in the XRD patterns of both a-Se and a- $\text{SeSm}_{0.005}$ remains undoubtedly visible in c- $\text{SeSm}_{0.008}$ in the range of the Bragg angles of $20^\circ \sim 23$ -32. In such halo diffraction range, the crystal

planes are reflected at the highest intensities in the diffraction pattern of c-SeSm_{0.008}. Subsequently, it is worth mentioning that the existence of a diffraction hump in the investigated deposited films of c-SeSm_{0.008} indicates that the matrix is not completely crystalline, as we call it crystallized sample; in other words, it reflects some degree of disordering in the sample matrix.

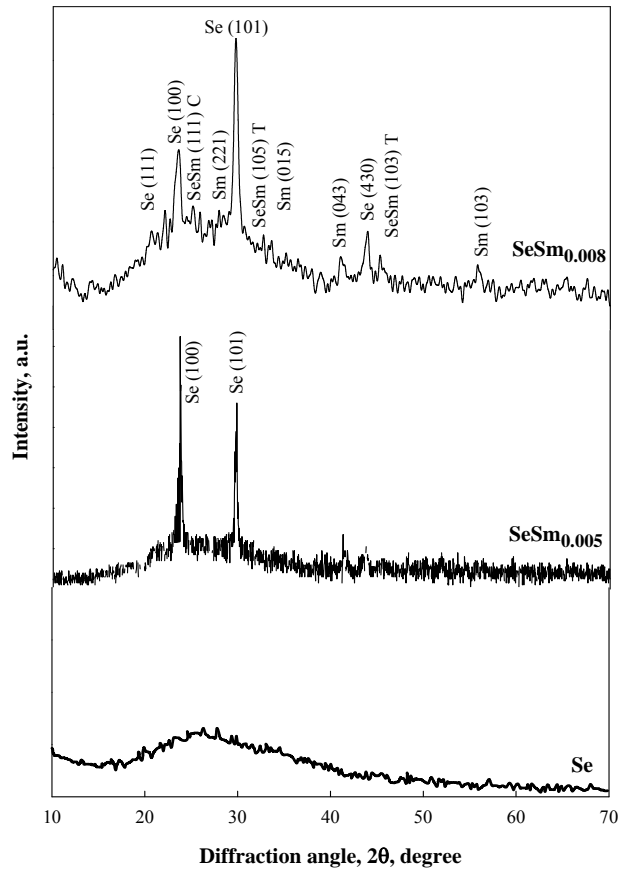


Fig. 1. XRD patterns of the as-prepared Se, SeSm_{0.005} and SeSm_{0.008}.

3.2. Optical constants and energy gap

Both of the optical constants, n (refractive index) and k (extinction coefficient), represent fundamental properties of a material not only because of their relation to the electronic structure but also due to their applications in many integrated optical devices. Thus, calculating n and k of a material are the key parameters for a device design (c.f., [23]). The optical constants, n and k , of semiconducting materials could be evaluated using a set of various optical methods (c.f., [24]). The $T(\lambda)$ recorded spectrum of the studied a-Se, a-SeSm_{0.005} and c-SeSm_{0.008} films are shown in Fig. 2 comparative to that of the glass substrate (T_s). In this figure, each studied film illustrates an interference pattern with fall of transmittance at the band edge. Due to such interference patterns, the method suggested by Swanepoel [25], represents a suitable model to calculate the two optical constants n and k as a function of λ . In fact, this method has been widely used to calculate interesting optical parameters of different chalcogenide films (c.f., [26-29]). The dispersion of n obeys, with a good approximation, Cauchy dispersion equation that has the form:

$$n = A + \frac{B}{\lambda^2} + \frac{C}{\lambda^4}, \quad (1)$$

where A , B and C are known as Cauchy coefficients that characterize the material investigated. The physical significance of these coefficients is given elsewhere [29]. Fig. 3 shows the calculated spectral dispersion of the real part of the complex refractive index ($\tilde{n} = n - ik$) for the three films investigated. In this figure, the dispersion of n demonstrates a monotonic decrease against λ . The decrease of n with λ is merely a common character for the chalcogenide semiconductors. However, the doping of 0.005 and 0.008 % Sm in a-Se leads to a reasonably respective decrease and increase in $n(\lambda)$ pertaining to that of pure a-Se. The relative increase of $n(\lambda)$ for 0.008 % Sm with respect to that of a-Se is accompanied by the crystallized character of the $\text{SeSm}_{0.008}$ film matrix, (see Fig.1). The absorption coefficient (α) of the investigated un-doped and two Sm doped Se films are calculated using the relation: $\alpha = 4\pi k / \lambda$, where k is the value of the extinction coefficient at a given λ . Fig. 4 displays a plot of α versus the photon energy $h\nu$, where h is Plank's constant. This figure points up the virtual rate of exponential increase of the function $\alpha = f(h\nu)$ as being accompanied by a corresponding shift to lower and higher energy values with the doping of a-Se with 0.005 and 0.008 % of Sm. Such a shift should indicate a non-monotonic change in the absorption edge of the compositions investigated.

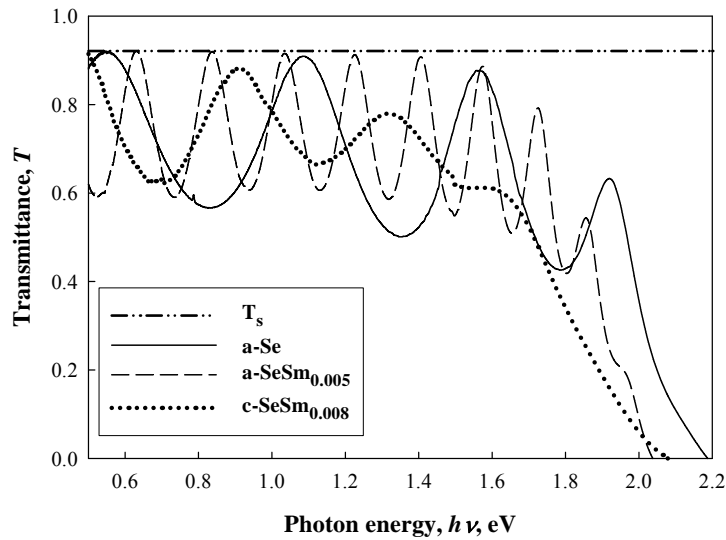


Fig. 2. Transmittance versus wavelength as recorded for the studied a-Se, a-SeSm_{0.005} and c-SeSm_{0.008} films. T_s refers to the transmittance of the quartz substrate.

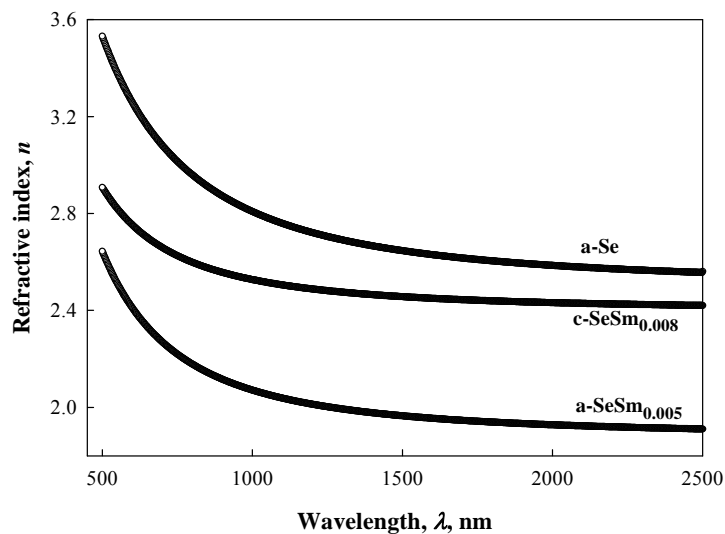


Fig. 3. Plots of the fitted refractive index versus wavelength for the films investigated.

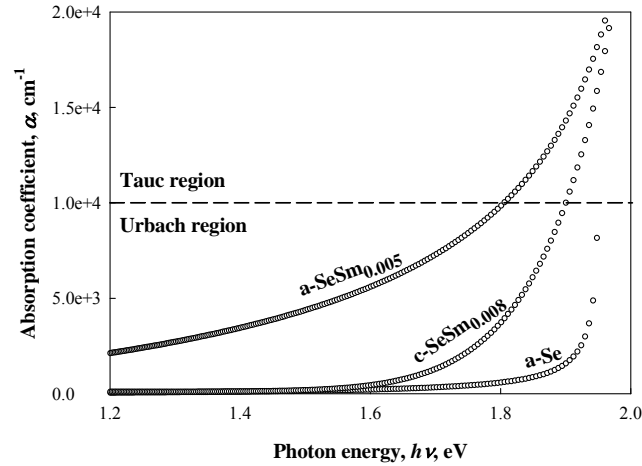


Fig. 4. The calculated absorption coefficient as a function of photon energy for the films investigated. The dashed line differentiates between the Tauc and Urbach regions.

Plot of the function $\alpha=f(h\nu)$ for each investigated composition that shown in Fig. 4, could be subdivided into two regions [30]:

The first region is for the higher values of the absorption coefficient, namely for $\alpha(h\nu)>10^4 \text{ cm}^{-1}$, that corresponds to transitions among extended states in both valence and conduction bands, where the power law of Tauc:

$$\alpha(h\nu)h\nu = A(h\nu - E_g)^2 \quad (2)$$

is valid for indirect transitions, where A is a constant. The functional dependence of the optical absorption coefficient $(\alpha h\nu)^{1/2}$ versus $h\nu$ is shown in Fig. 5 for the films investigated. For each composition, the energy gap (E_g) has been calculated by fitting the straight part in the high energy region of the function $(\alpha h\nu)^{1/2} = f(h\nu)$, locally point by point, to a linear regression line with fitting parameter $R^2 \approx 0.99$ and the results are given in Table 1. At this point, the value of E_g shows a decrease from 1.89 ± 0.018 to 1.70 ± 0.017 eV with the introduction of 0.005 % Sm into pure a-Se. The presentation of 0.008 % Sm to a-Se, that led to the formation of c-SeSm_{0.008}, corresponds to $E_g=1.77 \pm 0.018$ eV.

Table 1. The compositional dependence of the indirect optical energy gap (E_g), Urbach energy (E_u), high frequency dielectric constant (ϵ_∞), ratio of free carrier concentration to the free carrier effective mass (N/m^*), and plasma resonance frequency (ω_p).

Film Composition	E_g , eV	E_u , eV	ϵ_∞	N/m^* $\times 10^{49}$, $\text{cm}^{-3}\text{kg}^{-1}$	ω_p , $\times 10^{14}$, Hz
a-Se	1.89 ± 0.018	0.30	6.83	5.71	0.16
a-SeSm _{0.005}	1.70 ± 0.017	0.42	4.59	2.68	1.30
c-SeSm _{0.008}	1.77 ± 0.018	0.10	5.97	2.10	1.01

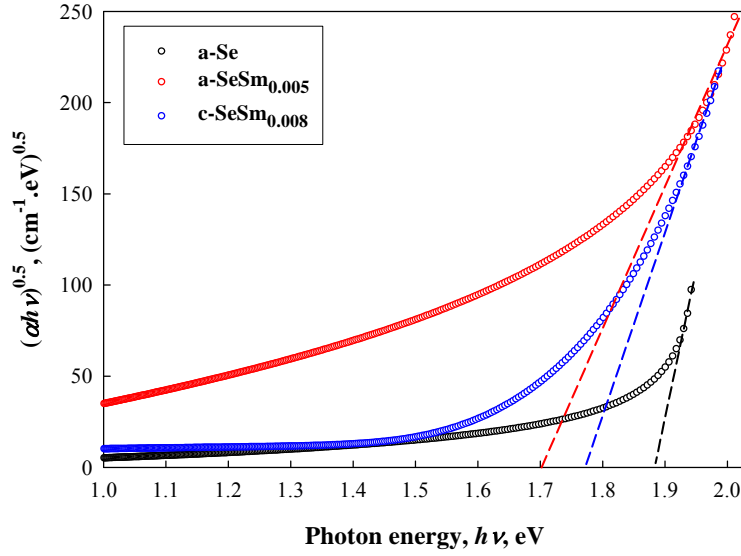


Fig. 5. Tauk's plots for determining the optical energy gap of indirect transitions for the films investigated.

The second region for $\alpha(h\nu)$ is for the lower values of α , that is for $\alpha(h\nu) < 10^4 \text{ cm}^{-1}$, where the absorption coefficient presents a roughly exponential behavior:

$$\alpha = \alpha_0 \exp(h\nu / E_u), \quad (3)$$

where the absorption in this region is due to transitions between extended states in one of the bands and localized states in the exponential tail of the other band [31]. The inverse slope, or the width of the exponential edge (E_u), reflects the width of the more extended band tail that is often called Urbach energy. Such exponential, or Urbach, edge is usually ascribed to localized states at the band edges. In other words, the Urbach edge is determined by the degree of disorder (e.g., charged impurities) and/or structural defects (e.g., broken or dangling bonds, vacancies, non-bridging atoms, or chain ends) in the considered semiconductor material [5]. The structural defects are collected together or assembled with impurities thus forming defect complexes in order to obtain a lower energy state. The calculated values of E_u are given in Table 1 as a function of film composition. These values show an increase from 0.30 eV for the un-doped (pure) a-Se film to 0.42 eV for the one doped a-Se sample with 0.005 % Sm. Such increase in the value of E_u indicates an increase in the disorder character of a-Se due to the introduction of Sm. This may be due to the formation of charged impurities and/or structural defects in the quasi-gap of a-SeSm_{0.005} than do in that of a-Se. Also, the fact that a-SeSm_{0.005} (1.70±0.017 eV) has smaller energy gap than a-Se (1.89±0.018 eV), implies that the formation of defects in the narrower gap will have more effect [32,33].

Conversely, increasing the Sm doping concentration to 0.008 % in a-Se leads to decreasing the width of the localized tail states to 0.1 eV. Such a decrease of E_u is attributed to the crystallized character of the thermally deposited SeSm_{0.008} film. Also, the presence of band tail (E_u) that accompanied the localized states in the gap reflects some degree of disorder in the considered semiconductor film. This last remark confirmed the existing hump in the Bragg's angle range of the strongest lines in the recorded XRD pattern of c-SeSm_{0.008} (see, Sec. 3.1 and Fig. 1).

3.3. Inter-band transitions

The non-monotonic trend of the function $E_g=f(\% \text{ Sm})$ that was observed, in Sec. 3.2, for the investigated films, could be explained regarding the effect of Sm-doping on the energy band structure of a-Se. In fact, many optical measurements are used to estimate the energy levels of Sm in the energy band of Sm doped-chalcogenides; these include: optical absorbance [2,34], optical density [17,35] and reflectance spectra [2,36]. Here, Fig. 6 explicates the $R(\lambda)$ spectra as automatically recorded for the films investigated. Each peak, in this figure, represents an optical transition that arises between two distinct energy states in the energy gap. Accordingly, for pure a-Se, there are four transitions occurring at energy values of 0.83, 1.39, 1.80 and 2.05 eV. The doping of a-Se with 0.005 % Sm leads to shift the first two transitions (0.83 and 1.39 eV) in case of a-Se to 0.73 and 1.32 eV, while the two other transitions (1.80 and 2.03 eV) remain unchanged. Besides these four transitions, there are other five ones appeared at 0.94, 1.13, 1.52, 1.62 and 1.92 eV. On the other hand, the increase of the Sm doping concentration to 0.008 % in a-Se, leads to a reduction in the number of possible optical transitions, whereas, only five ones turned up to be out of the nine transitions in case of the emergence of a-SeSm_{0.005}; these cropped up at energy values of 0.71, 1.13, 1.49, 1.80 and 2.07 eV.

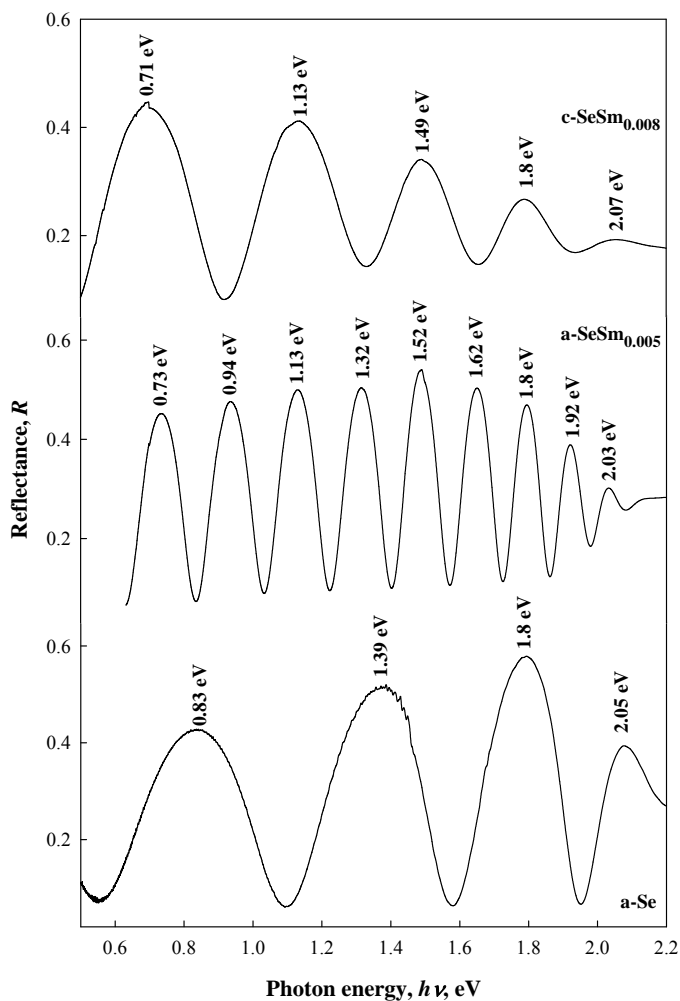


Fig. 6. Reflectance versus photon energy for the studied films with the numerical transition energy value of each recorded peak.

3.4. Dispersion of the optical dielectric constant

The complex dielectric function describes the interaction between the electromagnetic waves and the matter. The complex dielectric (ϵ) constant of a material is given in terms of the real (n) and imaginary (k) parts of the complex refractive index \tilde{n} as: $\epsilon_1 = n^2 - k^2$, where ϵ_1 is the real part of the complex dielectric constant, while the imaginary part is given by $\epsilon_2 = 2nk$. These two parts are shown in Fig. 7(a,b) for the films investigated. For all compositions, the imaginary dielectric constant shows an exponential increase with $h\nu$. Such an increase is accompanied by a shift towards higher photon energy for a-SeSm_{0.005} and a shift to lower energies for c-SeSm_{0.008}. This refers, of course, to that the level of Sm concentration (0.0-0.008 % Sm) in a-Se matrix, and hence the nature of the formed thermally deposited films (amorphous embedded with some crystalline zones, a-SeSm_{0.005}, or crystalline embedded with some amorphous zones, c-SeSm_{0.008}), leading to the effect of the free carriers density, assuming that the free carrier effective mass (m^*) is constant.

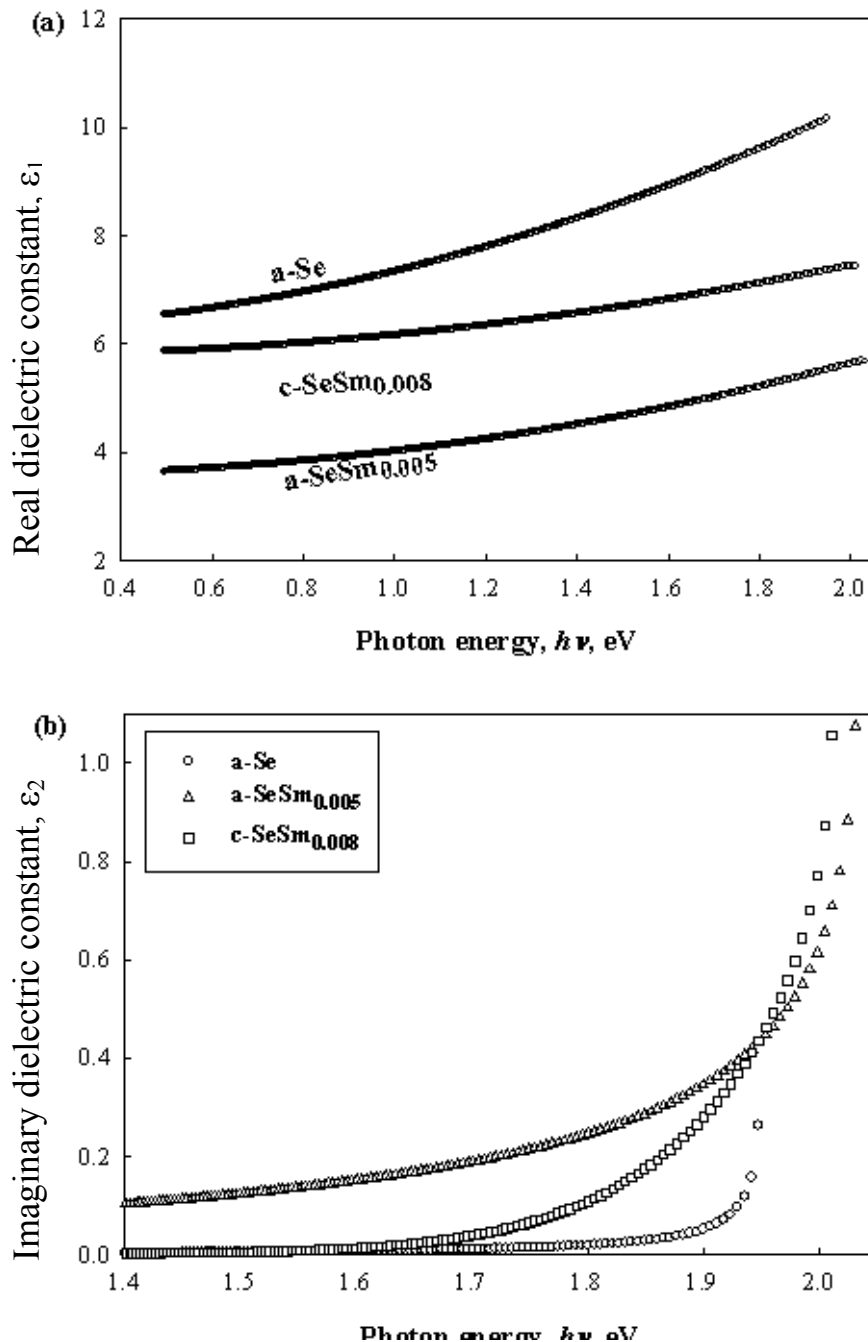


Fig. 7. Imaginary (a) and real (b) parts of the dielectric constant versus photon energy for the films investigated.

In the region of relatively high wavelength, the real part of the dielectric constant (ϵ_1) can be written as [37]:

$$\epsilon_1 = \epsilon_\infty - \frac{e^2}{4\pi^2 c^2 \epsilon_o} \frac{N}{m^*} \lambda^2, \quad (4)$$

where, $\frac{N}{m^*} = \frac{\epsilon_o \epsilon_\infty}{e^2} \omega_p^2$

Here, ω_p is the plasma resonance frequency of all the valence electrons involved in the optical transitions, ϵ_∞ the high frequency dielectric constant, e electronic charge, c velocity of light, ϵ_o free space dielectric constant and N/m^* is the ratio of free carriers density to the free carrier effective mass. According to Eq. (4), the slope and intercept of the graphical presentation of the function $\epsilon_1 = f(\lambda^2)$, yield the respective values of both N/m^* and ϵ_∞ . Values of the former are used to calculate ω_p . The evaluated values of ϵ_∞ , N/m^* and ω_p are given in Table 1 as a function of film composition. The value of N/m^* reflects a monotonic decrease in the free carrier density with the introduction of up to 0.008 % Sm to a-Se. Also, Table 1 indicates that the wavelength $\lambda_{\omega=\omega_p}$, corresponded to the plasma frequency ω_p , and evaluated from the relation $2\pi c/\omega_p$, shows a shift towards shorter wavelengths ($\sim 1.2 \times 10^5 - 1.4 \times 10^4$ nm) with the doping of 0.005 % Sm in a-Se, while the shift towards higher wavelengths (1.8×10^4 nm) in case of c-SeSm_{0.008}.

Also, the model proposed by Wemple and DiDiomenico [38] could be applied, at this instant, to describe the optical transitions for the Se-Sm films investigated. In this model, the refractive index data have been examined below the inter-band absorption edge, where the normal dispersion of the optical dielectric constant of the material and the energy dependence of refractive index satisfy the following relation:

$$n^2 - 1 = \frac{E_o E_d}{E_o^2 - (h\nu)^2} \quad (5)$$

where E_o is the average oscillator energy and E_d is the dispersion energy parameter of the material that measures the strength of inter-band optical transitions. The parameter E_d is related to the nearest neighbor cation coordination, anion valence, ionicity as well as the effective number of dispersion electrons, [39]. For materials containing $f \rightarrow d$ transitions, such as the present case of rare earth element (Sm) doped Se films, Eq. (5) could be rewritten as:

$$n^2 - 1 = \frac{\hat{E}_d \hat{E}_o}{\hat{E}_o^2 - (h\nu)^2} + \frac{E_d E_o}{E_o^2 - (h\nu)^2} \quad (6)$$

where \hat{E}_d, \hat{E}_o applies to $f \rightarrow d$ transitions, due to doping with Sm, and E_d, E_o applies to $s, p \rightarrow d$ transitions of Se. Equating the right hand sides of Eqns. (5 & 6) and solving yields:

$$\bar{E}_o^2 = \hat{E}_o^2 \left(\frac{1 + (E_d / \hat{E}_d)(\hat{E}_o / E_o)}{1 + (E_d / \hat{E}_d)(\hat{E}_o / E_o)^3} \right) \quad (7)$$

and $\bar{E}_d^2 = \hat{E}_o^2 \left(\frac{[1 + (E_d / \hat{E}_d)(\hat{E}_o / E_o)]^3}{1 + (E_d / \hat{E}_d)(\hat{E}_o / E_o)^3} \right)$

where \bar{E}_o and \bar{E}_d are the average values of the single oscillator energy and dispersion energy, respectively. According to Eq. (6), plots of $(n^2 - 1)^{-1}$ versus $(h\nu)^2$ are shown in Fig. 8 for the three compositions investigated. Fitting the straight part of each plotted curve in the high energy region allows one to obtain the values of both E_o and E_d given in Table 2. The values of \hat{E}_d and \hat{E}_o were

calculated by fitting the straight part of the same curves in the low photon energy region and given in Table 2 along side the film composition.

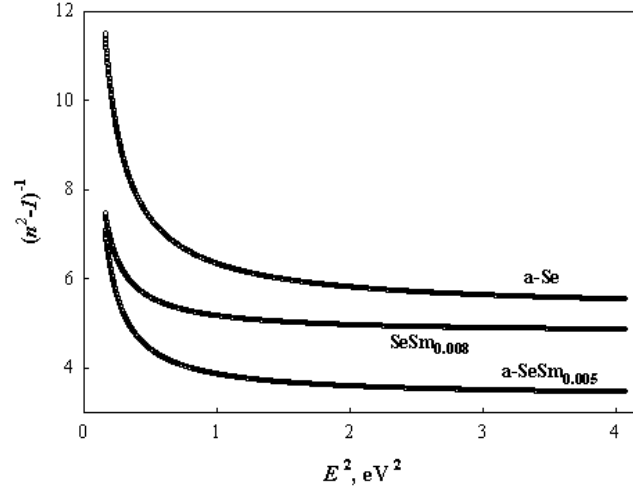


Fig. 8. Plots of $(n^2-1)^{-1}$ versus $(hv)^2$ for the films investigated.

Table 2. The single oscillator energy (E_o, \bar{E}_o), dispersion energy (E_d, \bar{E}_d), lattice oscillator strength (E_l), and wavelength at zero material dispersion (λ_c) as a function of film composition.

Film Composition	E_o , eV	E_d , eV	\hat{E}_o , eV	\hat{E}_d , eV	\bar{E}_o , eV	\bar{E}_d , eV	E_l , eV	λ_c , μm
a-Se	4.00	28.65	---	---	4.00	---	0.38	2.1593
a-SeSm _{0.005}	3.74	12.62	2.49	6.34	3.00	7.02	0.54	1.8937
c-SeSm _{0.008}	4.50	23.50	3.58	17.10	3.97	8.36	0.36	1.6415

In view of that, the estimated value of E_o for a-Se (4.0 eV) is in good agreement with that reported by Wemple [40]. The results indicated that the average value of the single oscillator energy (\bar{E}_o) changed to 3.0 eV for a-SeSm_{0.005} and to 3.97 eV for c-SeSm_{0.008}, Table 2. Such non-monotonic behavior of \bar{E}_o could be attributed to the splitting of the sub-bands $5d(t_{2g}-e_g)$ by the crystal field in a-SeSm_{0.005}, and the decrease of this splitting as well as the crystallized nature with increasing Sm-content in c-SeSm_{0.008}.

In fact, the two optical energy parameters E_o and E_d are related to another interesting optical parameter known as the lattice oscillator strength (E_l) by the relation [41,42]:

$$n^2 - 1 = \left(\frac{\hat{E}_d \hat{E}_o}{\hat{E}_o^2 - E^2} + \frac{E_d E_o}{E_o^2 - E^2} \right) - \frac{E_l^2}{E^2} \quad (8)$$

At long wavelengths, where $(hv)^2 \ll E_o^2$, Eqn. (8) tends to be:

$$n^2 - 1 = \left(\frac{\hat{E}_d}{\hat{E}_o} + \frac{E_d}{E_o} \right) - \frac{E_l^2}{E^2} \quad (9)$$

That is, a plot of $(n^2 - 1)$ versus $1/(hv)^2$ approaches a straight line whose an intercept equals $\{(\hat{E}_d/\hat{E}_o)+(E_d/E_o)\}$ and slope is $-E_i^2$. Here, it is worth mentioning that the magnitude of the intercept is in quite good agreement with that when substituting the corresponding values of E_d and E_o , given in Table 2, in its mathematical form. The obtained values of E_i are given in Table 2, as well stating a variation from 0.38 eV for a-Se to 0.54 eV and 0.36 eV for a-SeSm_{0.005} and c-SeSm_{0.008}, respectively.

Using the values of E_i together with those of E_d (\bar{E}_d) and E_o (\bar{E}_o), one can calculate the material dispersion $M(\lambda)$ parameter, defined as [43]:

$$M(\lambda) = \frac{\lambda}{c} \left(\frac{d^2 n}{d\lambda^2} \right) \quad (10)$$

that can be obtained by differentiating twice Eq. (8) with respect to λ . Hence, Fig. 9 shows a plot of the function $M(\lambda)=f(\lambda)$. Hence, one can use this figure to find out the wavelength value λ_c , at which $M(\lambda)=0$, and the obtained results are given in Table 2 as a function of film composition. Similarly, the value of λ_c can be calculated from the Wemple's three-parameter formula [43]:

$$\lambda_c = 1.63 \left(\frac{\bar{E}_d}{\bar{E}_o^3 \bar{E}_i^2} \right)^{\frac{1}{4}} \quad (11)$$

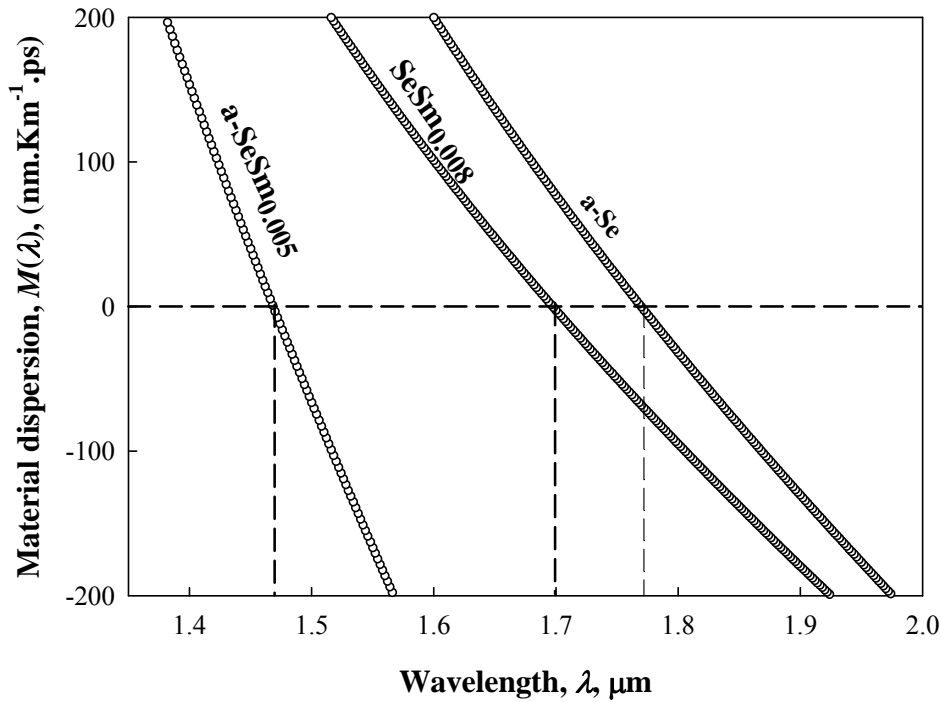


Fig. 9. Plots of the material dispersion versus wavelength for the films investigated

Consequently, it is worth noting that the values of λ_c that computed from Fig. (9) or from Eq. (11) are in conformity with that indicating a monotonic shift of λ_c towards lower wavelengths with the introduction of up to 0.008 % Sm in a-Se (Table 2). In fact, a shift in λ_c represents an important factor in determining the operational conditions and performance of optical fibers, [44].

4. Conclusions

An extensive investigation for the role that the doping of Sm, up to 0.008 %, plays in manipulating the optical characteristic parameters of pure a-Se, applying the current optical

theories and models on the recorded $T(\lambda)$ and $R(\lambda)$ spectra, bringing about the foremost subsequent two remarks:

* A monotonic decrease for the estimated values of the free carrier density (N) and the wavelength at zero material dispersion (λ_c) with the introduction of up to 0.008 % Sm to a-Se.

* A similar non-monotonic trend, whether towards lower or higher wave-lengths, for the Sm-doping concentration of the two components of the complex dielectric constant (ϵ_1 and ϵ_2), dispersion refractive index (n), optical energy gap of indirect transitions (E_g), Urbach energy (E_u), lattice oscillating strength (E_l) as well as for the single oscillator energy (E_o).

References

- [1] R. Suryanarayanan, C. Paparoditis, *J. Appl. Phys.* **43** 4105 (1972).
- [2] E. Kaldis, P. Wachter, *Sol. Stat. Commun.* **11** 907 (1972).
- [3] T. Le Bihan, S. Darracq, S. Heathman, U. Benedict, K. Mattenberger, O. Vogt, *J. Alloy. Compd.* **226** 143 (1995).
- [4] W. Suski, *Phys. Status Solidi* **41** 733 (1999).
- [5] N.F. Mott, E.A. Davis, *Electronic Processes in Non-Crystalline Materials*, Clarendon Press, Oxford, 1979.
- [6] S.R. Elliott, *Physics of Amorphous Materials*, John Wiley & Sons, New York, 1990.
- [7] M.F. Kotkata, *J. Mater. Sci.* **27** 4847 (1992); *ibid*, **27** 4858 (1992).
- [8] M.F. Kotkata, D.Sc. Thesis, Transport and Structural Properties of Non-Crystalline Chalcogenide Semiconductors, Hungarian Academy of Sciences, Budapest, 1993.
- [9] I.V. Prots, V.K. Malinovsky, N.V. Surovtsev, *Glass Phys. Chem.*, **34** 30 (2008).
- [10] V.N. Antonov, B.N. Harmon, A.N. Yareska, *Phys. Rev.* **B 66** 165208 (2002).
- [11] H.S. Wio, B. Aloscio, A. López, *Sol. Stat. Commun.* **15** 1933 (1974).
- [12] A. Svane, G. Santi, Z. Szotek, W.M. Temmerman, P. Strange, M. Horne, G. Vaitheeswaran, V. Kanchana, L. Petit, H. Winter, *Phys. Status Solidi* **B 241** 3185 (2004).
- [13] P.K. Dwivedi, Y.W. Sun, Y.Y. Tsui, D. Tonchev, M. Munzar, K. Koughia, C.J. Haugen, R.G. DeCorby, N. McMullin, S.O. Kassap, *Appl. Surf. Sci.* **248** 376 (2005).
- [14] V.S. Shiryayev, C. Boussard-Pl'Edel, P. Houizot, T. Jouan, J.L. Adam, J. Lucas, *Mater. Sci. Eng.* **B 127** 138 (2006).
- [15] J. Teteris *Curr. Opin. Solid State Mater. Sci.* **7** 127 (2003).
- [16] J.S. Sanghera, I.D. Aggarwal, *J. Non-Cryst. Solids*, 256–257 (1999) 6.
- [17] C. Paparoditis, R. Suryanarayanan, *J. Cryst. Growth* **13/14** 389 (1972); *ibid*, *Phys. Lett.* **42** 373 (1973).
- [18] A.K. Singh, B.M.S. Bist, P.N. Srivastava, *Thin Solid Films*, **35** L11 (1976).
- [19] S.B. Jundale, C.D. Lokhande, *Mater. Chem. Phys.* **38** 325 (1994).
- [20] F.A. Abdel-Wahab, H.M. Maksoud, M.F. Kotkata, *J. Phys. D: Appl. Phys.* **39** 190 (2006).
- [21] M.F. Kotkata, F.A. Abdel-Wahab, H.M. Maksoud, *J. Phys. D: Appl. Phys.* **39** 2059 (2006).
- [22] R.B. Bekeen, J.W. Schweitzer, *Phys. Rev.* **B 23** 3620 (1981).
- [23] V. Pamuckchieva, A. Szekeres, *Optical Mater.* **30** 1088 (2008).
- [24] S. Boycheva, A. Krasilnikova Sytchkova, J. Bulir, C. Popov, W. Kulisch, A. Piegari, *J. Non-Cryst. Solids* **353** 1618 (2007).
- [25] R. Swanepoel, *J. Phys. E: Sci. Instrum.* **16** 1214 (1983); *ibid*, **17** 896 (1984).
- [26] E. Marquez, J. Ramirez-Malo, P. Villares, R. Jimenez-Garay, P.J.S. Ewen, A.E. Owen, *J. Phys. D: Appl. Phys.* **25** 535 (1992).
- [27] M.F. Kotkata, H.T. El-Shair, M.A. Afifi, M.M. Abdel-Aziz, *J. Phys. D: Appl. Phys.* **25** 535 (1992).
- [28] P. Sharma, V. Sharma, S.C. Katyal, *Chalcogenide Lett.* **3** (2006) 73.
- [29] M.F. Kotkata, F.A. El-Wahab, M.S. Al-Kotb, *Appl. Surf. Sci.* **255** 9071 (2009).
- [30] J. Tauc, *Amorphous and Liquid Semiconductors*, Plenum, New York, 1974; *ibid*, *Phys. Status Solidi* **15** 627 (1996).
- [31] M.H. Cohen, C.M. Soukoulis, E.N. Economou, *AIP. Conf. Proc.* **120** (1984).
- [32] M.H. El-Fouly, M.F. Kotkata, A.Z. El-Behay, M.A. Morsy, *Radiat. Phys. Chem.* **23** 553 (1984).

- [33] M.F. Kotkata, M.H. El-Fouly, S.A. Fayek, S.A. El-Hakim, *Semicond. Sci. Technol.* **1** 313 (1986).
- [34] G.V. Lashkarev, L.A. Ivanchenko, *J. Non-Cryst. Solids* **8-10** 670 (1972).
- [35] R. Suryanarayanan, C. Paparoditis, J. Ferré, B. Briat, *J. Appl. Phys.* **43** 4105 (1972).
- [36] A. Kurita, Y. Kaneko, T. Koda, *Sol. Stat. Commun.* **49** 463 (1984).
- [37] T.S. Moss, G.J. Burrell, E. Ellis, *Semiconductor Opto-Electronics*, Butterworths, London, 1973.
- [38] S.H. Wemple, M. DiDomenico, *Phys. Rev.* **B 3** 1338 (1971).
- [39] J.R. Bell, M.A. Ordal, R.W. Alexander, *Appl. Opt.* **24** 3680 (1985).
- [40] S.H. Wemple, *Phys. Rev.* **B 7** 3767 (1973).
- [41] H. Poignant, *Electron. Lett.* **17** 973 (1981).
- [42] M.Y. Han, H. Huang, C.H. Chew, X.J. Zhang, W. Ji, *J. Phys. Chem.* **B 102** 1884 (1998).
- [43] S.H. Wemple, *Appl. Opt.* **18** 31 (1979).
- [44] R.W. Boyd, *Nonlinear Optics*, Academic Press, 1992.